

# Benchmark Simulations of Flow Past Moving Rigid Bodies Using a Sharp Interface Immersed Boundary Method

U. Senturk<sup>1</sup>, D. Brunner<sup>2</sup>, N. Herzog<sup>2</sup>, H. Jasak<sup>3</sup>, C. W. Rowley<sup>4</sup>, A. J. Smits<sup>4,5</sup>

<sup>1</sup> Department of Mechanical Engineering, Ege University, Izmir 35040, Turkey

<sup>2</sup> ZHAW Zurich University of Applied Sciences, Winterthur 8401, Switzerland

<sup>3</sup> Faculty of Mechanical Engineering and Nav. Arch., University of Zagreb, Zagreb 10000, Croatia

<sup>4</sup> Department of Mechanical and Aerospace Eng., Princeton University, Princeton 08544, USA

<sup>5</sup> Department of Mechanical and Aerospace Eng., Monash University, Victoria 3800, Australia

Corresponding author: utku.senturk@ege.edu.tr

**Abstract:** This study reports selected benchmark results of an IBM based finite volume solver within the framework of the open source toolbox *foam-extend 3.2*. The immersed boundary formulation uses a discrete forcing approach based on a weighted least squares approximation that preserves the sharpness of the boundary. In this context, we present two test cases: (1) a 2D cylinder which oscillates transversely at a flow Reynolds number of 185, and (2) a 3D, rigid plate that pitches about its leading edge at a Reynolds number of 2000. Preliminary force coefficient results are compared with available computational and experimental data. In addition, a snapshot POD analysis was performed on the pitching plate problem to reveal the energetic modes and to identify the large-scale structure of the wakes.

*Keywords:* Computational Fluid Dynamics, Immersed Boundary Method, Discrete, Oscillating Cylinder, Pitching Plate.

## 1 Introduction

Immersed boundary methods (IBMs) have been successfully employed in simulation of fluid problems as an alternative to boundary-fitted methods, particularly in problems involving interactions with moving boundaries. IBMs refer to a family of methods that may be classified broadly as either continuous or discrete forcing approaches [1]. The computational fluid dynamics (CFD) code that is used in this work is a recently released, open-source, IBM based finite volume solver *foam-extend 3.2* [2, 3]. It is an extension to the open-source continuum mechanics solver OpenFOAM (FOAM: Field Operation and Manipulation). The code treats the immersed boundaries using the discrete approach, and the boundary conditions on rigid walls are enforced by a weighted least squares procedure to preserve the sharpness of the body contour. For the ultimate purpose of having a computational tool to simulate flow around fish-like bodies, a detailed benchmarking study was performed. Here, we present two cases, namely, a two-dimensional, transversely oscillating cylinder at a Reynolds number  $Re = U_\infty D/\nu = 185$  and a three-dimensional pitching plate about its leading edge at a Reynolds number  $Re = U_\infty c/\nu = 2000$ . Here,  $U_\infty$  is the freestream velocity,  $D$  is the cylinder diameter,  $c$  is the plate chord, and  $\nu$  is the fluid kinematic viscosity.

## 2 IBM Capabilities in FOAM

An extension to the open-source toolbox OpenFOAM called *foam-extend 3.2* is used in this work. Current release of the code features the IBM capability for a range of flows involving turbulence modeling and multiphase flows. The primary interest in this work is to setup a simulation environment to study underwater locomotion for low Reynolds numbers. Thus, we focus on unsteady, laminar, incompressible external flows where a body in motion exists in a free stream of flow. For such simulations a new solver *icoDyMIbFoam* obtained by modifying the previously existing solver *icoFoam* by the additional IBM libraries. Such modifications will be addressed briefly herein.

The conservative form of the continuity and Navier-Stokes equations under the assumptions of unsteady, laminar, incompressible flow are

$$\frac{\partial \mathbf{V}}{\partial t} + \nabla \cdot (\mathbf{V}\mathbf{V}) - \nabla \cdot (\nu \nabla \mathbf{V}) = -\nabla p \quad (1)$$

$$\nabla \cdot \mathbf{V} = 0 \quad (2)$$

where  $\mathbf{V}$ ,  $p$  and  $\nu$  represent the velocity field, kinematic pressure field and kinematic viscosity. The latter is converted to a Poisson equation for pressure. Within the context of FOAM, these equations are discretized with a finite-volume approach where an integration is applied throughout the non-overlapping polyhedral cells of the flow domain. This is followed by the conversion into surface integrals (by Gauss theorem) and eventually discrete surface fluxes. In the current solver, the pressure-velocity coupling is handled by the PISO (Pressure Implicit with Splitting of Operator) algorithm. Details of the numerics can be found in [2] and [3].

The immersed boundary solver requires a background grid and an immersed boundary (IB) surface defined by the user. The IB surface is introduced as an STL (STereoLithography) file which involves the triangulated IB grid data. At each time step of an unsteady flow around a moving body, the code tags the cells as fluid, IB, or solid cells. The boundary conditions (BCs) to be enforced on the IB surface are introduced by assigning appropriate values to the variables in IB cells. These values are found from a weighted least squares (WLS) interpolation. It is this interpolation that ensures a sharp representation of the IB.

For BCs, a multivariable quadratic interpolation is performed using the cells that fall within the region of influence defined by a circle around each IB cell. In the context of WLS, the summation  $\sum_{i=1}^n w_i (\phi_i - \tilde{\phi}_i)^2$  is minimized for  $n$  cells in the interpolation stencil for a given variable  $\phi$ . For the Dirichlet BC, interpolation in 2D reads

$$\tilde{\phi}_i = \phi_{ibp} + C_0 X_i + C_1 Y_i + C_2 X_i Y_i + C_3 X_i^2 + C_4 Y_i^2 \quad (3)$$

where  $X_i = x_i - x_{ibp}$  and  $Y_i = y_i - y_{ibp}$ . Here, the index  $i$  represents the  $i$ th cell in the interpolation stencil, and the index  $ibp$  represents the point on the IB surface which is closest to the IB cell that owns the stencil. The unknown coefficients are found by  $\mathbf{C} = (\mathbf{M}^T \mathbf{W} \mathbf{M})^{-1} \mathbf{M}^T \mathbf{W} \mathbf{A}$ , where the entries of the vector  $\mathbf{A}$  are  $\tilde{\phi}_i - \phi_{ibp}$ . Therefore the design matrix is built solely on the geometric information as,

$$\mathbf{M} = \begin{bmatrix} X_1 & Y_1 & X_1 Y_1 & X_1^2 & Y_1^2 \\ X_2 & Y_2 & X_2 Y_2 & X_2^2 & Y_2^2 \\ \dots & \dots & \dots & \dots & \dots \\ X_n & Y_n & X_n Y_n & X_n^2 & Y_n^2 \end{bmatrix} \quad (4)$$

and the corresponding weights are the diagonal element of the weight matrix  $\mathbf{W}$  are defined by

$$w_{ii} = \frac{1}{2} \left[ 1 + \cos \left( \pi \frac{r_i}{S r_{max}} \right) \right] \quad (5)$$

where  $S$  is a tweaking parameter and  $r$  is the local parameter that collects the distances between the stencil cells and the owner IB cell. Once the coefficients are found, the value in the IB cell is interpolated by substituting the owner IB cell coordinates in Eq. 3.

Neumann BCs are imposed in a similar fashion. For the pressure interpolation in 2D,

$$p_i = C_0 + C_1 X_i + C_2 Y_i + C_3 X_i Y_i + C_4 X_i^2 + C_5 Y_i^2 \quad (6)$$

Normal gradient of pressure can be written in terms of the tri-face normal  $\mathbf{n} = (n_x, n_y)$  as,

$$\frac{\partial p}{\partial n} = \frac{\partial p}{\partial x} n_x + \frac{\partial p}{\partial y} n_y \quad (7)$$

Here the partial derivatives are obtained by differentiating Eq. 6. Augmenting the design matrix by one row for the pressure gradient term gives,

$$\mathbf{M} = \begin{bmatrix} 1 & X_1 & Y_1 & X_1 Y_1 & X_1^2 & Y_1^2 \\ 1 & X_2 & Y_2 & X_2 Y_2 & X_2^2 & Y_2^2 \\ \dots & \dots & \dots & \dots & \dots & \dots \\ 1 & X_n & Y_n & X_n Y_n & X_n^2 & Y_n^2 \\ 0 & n_x & n_y & n_x Y_{ibp} + n_y X_{ibp} & 2n_x X_{ibp} & 2n_y Y_{ibp} \end{bmatrix} \quad (8)$$

Similarly, vector  $\mathbf{A}$  which collects the pressure values in the stencil cells now is augmented to include the pressure gradient value as

$$\mathbf{A} = [p_1 \ p_1 \ \dots \ p_n \ \partial p / \partial n]^T \quad (9)$$

Default weights for the Neumann BC imposition are

$$w_{ii} = 1 - \frac{r_i}{Sr_{max}} \quad (10)$$

After computing the coefficients, pressure value in the IB cell is found by Eq. 6.

Motion of the immersed boundary is handled using the dynamics mesh libraries. Prescribed motions are hooked by defining a function for the position vector ( $\mathbf{x}_{ib}$ ). The value of the Dirichlet BC on the IB is updated by

$$\mathbf{V}_{ib} = \frac{\mathbf{x}_{ib} - \mathbf{x}_{ib,old}}{\Delta t} \quad (11)$$

at each time step.

### 3 Validation Cases and Results

Two test problems visited within the current scope of this study are the oscillating cylinder and the pitching plate problems. The open-source *snappyHexMesh* utility is used to generate a non-uniform grid in a sufficiently large rectangular domain enclosing the IB. Multiple levels of refinement are generated so that the background grid size in the finest sub-domain around the IB is equal to the grid size on the IB. Typical boundary conditions are shown in Figure 1 for the 3D pitching plate problem. For the 2D oscillating cylinder same BCs apply except the front and back planes which are set as empty. All cases are initialized with the solver *potentialIbFoam* (potential flow solver with IB support) to prevent divergence at the start-up. Cell CFL numbers are kept below 0.5 by setting the time step appropriately in each problem.

#### 3.1 2D Flow Past a Transversely Oscillating Cylinder

We perform 2D simulations of a transversely oscillating cylinder located in a relatively large rectangular domain defined by corners  $(-15D, -15D)$  and  $(35D, 15D)$ . Uniform freestream velocity is  $U_\infty$ . Instantaneous position of the cylinder is defined by

$$y(t) = A \sin(2\pi t/T) \quad (12)$$

The grid size on the cylinder is  $\Delta s = 0.01D$ . Four levels of refinement are created around the cylinder

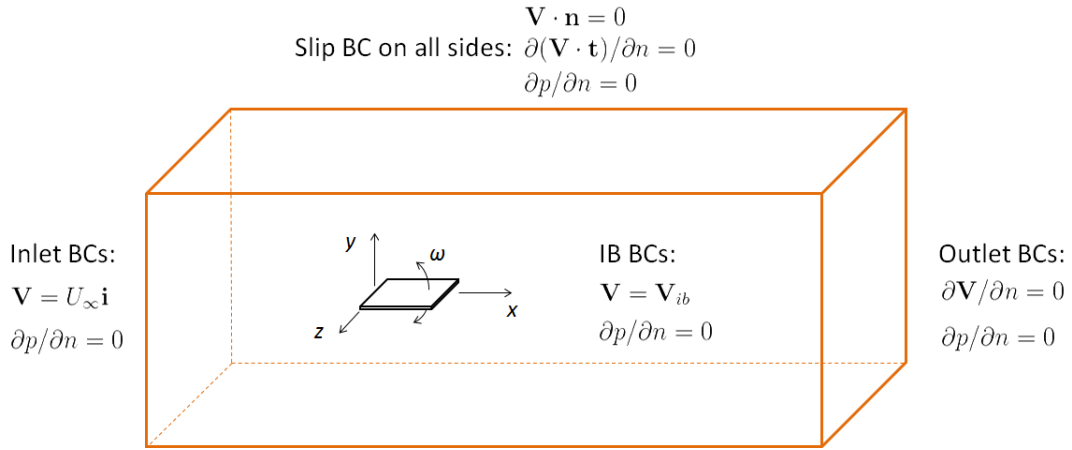


Figure 1: Domain and boundary conditions for the pitching plate problem ( $\omega$ : angular frequency).

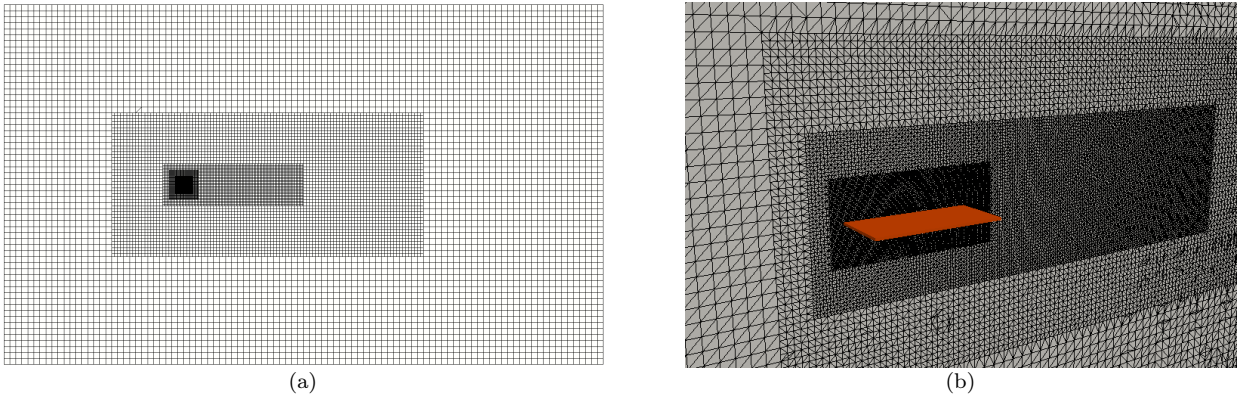


Figure 2: Views of the nested, unstructured grids created with the snappyHexMesh utility: (a) Cylinder problem (coarsened for better view), (b) Plate problem.

(Figure 2a). Instantaneous drag ( $C_D = F_D/\frac{1}{2}\rho s c U_\infty^2$ ) and lift ( $C_L = F_L/\frac{1}{2}\rho s c U_\infty^2$ ) coefficients are recorded. The relevant parameters of the problem are the Reynolds number, excitation amplitude scaled by diameter,  $A/D$ , and the excitation frequency scaled by the vortex shedding frequency of a fixed cylinder,  $f_e/f_0$ . We consider the cases with  $Re_D = 185$ ,  $A/D = 0.2$  and  $0.8 \leq f_e/f_0 \leq 1.2$  to reproduce the results presented in [4]

Figure 3 shows the temporal variations of the force coefficients. The curves are in qualitative agreement with previous findings [4]. In general, spurious oscillations are found in force signals which become more pronounced as frequencies get smaller. This is usually observed in IBM based computations which is attributed to the cells that change their flags from solid to fluid. Several algorithms were proposed ([5], [6]), however, current version of the code lacks such treatment.

In Figure 4a, time-averaged force coefficients are shown in comparison with the results from [4]. A good agreement is obtained with slightly higher drag for all frequencies investigated.

### 3.2 3D Flow Past a Pitching Plate

In this validation case, we introduce three-dimensionality by considering the flow past a pitching rectangular plate about its leading edge. The plate has a thickness of  $0.037c$ . The box domain enclosing the body is defined by the corners  $(-2c, -2.5c, -2.5c)$  and  $(6c, 2.5c, 2.5c)$ . Three levels of refinement are created (Figure 2b). Prior mesh convergence study showed that a grid size of  $\Delta s = 0.0125c$  in the finest subdomain yields

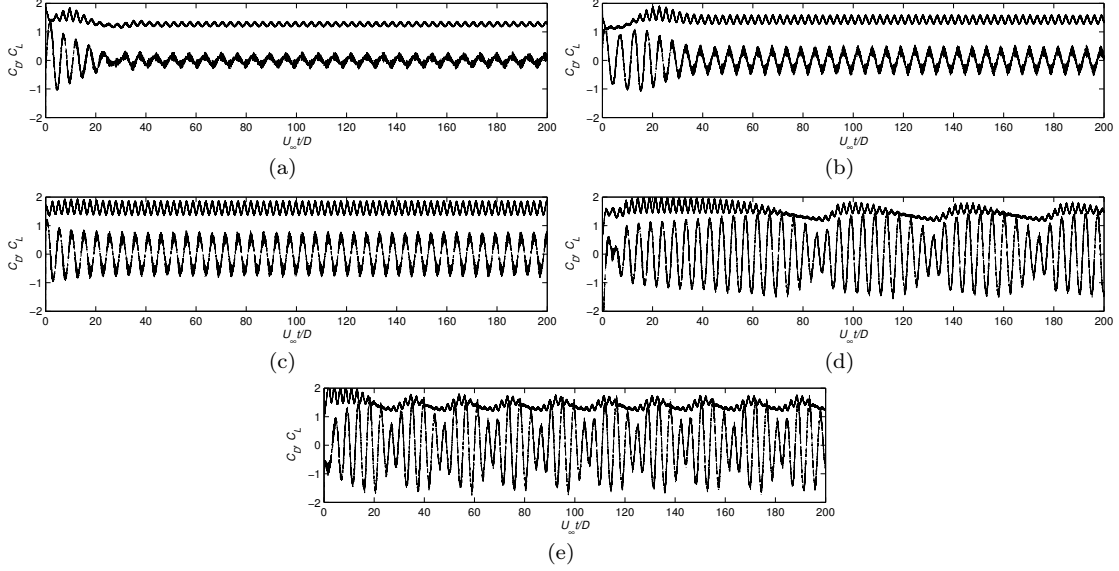


Figure 3: Temporal variation of the force coefficients for the oscillating cylinder case at  $Re_D = 185$ : (a)  $f_e/f_0 = 0.8$ , (b)  $f_e/f_0 = 0.9$ , (c)  $f_e/f_0 = 1.0$ , (d)  $f_e/f_0 = 1.1$ , (e)  $f_e/f_0 = 1.2$ . Upper curves in figures correspond to  $C_D$ .

sufficient accuracy to capture important aspects of the flow. The Reynolds number is set to  $Re_c = 2000$ . The wake structure and its relation to the forces exerted on the fluid by the propulsor is of major concern. The net thrust ( $F_T$ ) produced by the motion is non-dimensionalized as the thrust coefficient,

$$C_T = \frac{F_T}{\frac{1}{2}\rho s c U_\infty^2} \quad (13)$$

where  $s$  is the span. Propulsive performance is represented by the characteristic curve of  $C_T$  as a function of the Strouhal number based on the wake width ( $A_w$ ),

$$St = \frac{f A_w}{U_\infty} \quad (14)$$

where  $A_w$  is often assumed to be the peak-to-peak amplitude of the trailing edge which will be adopted here. The pitching motion is defined by the angle between the streamwise direction and the chord as,

$$\beta(t) = \beta_{max} \sin(2\pi t/T) \quad (15)$$

Results are compared with experiments performed in a water channel used by Dewey *et al.* [7], where a more complete description of the apparatus may be found. The angle  $\beta_{max}$  is fixed to  $8^\circ$  and the frequency is varied to change the Strouhal number. Figure 4b compares the time-averaged thrust ( $\overline{C_T}$ ) computations with experiments. The numerical results are generally a little higher than the experimental data, and the agreement seems to improve with Strouhal number. It is also noted that the anticipated quadratic behaviour of  $\overline{C_T}$  is obtained in the simulations.

Iso-surfaces of non-dimensional vorticity magnitude are shown in Figure 5. Two plots correspond to the same Reynolds number ( $Re_c = 2000$ ) but different Strouhal numbers ( $St=0.2$  and  $St=0.4$ ). These Strouhal numbers belong to two distinct wake states where 2S type wakes are observed in the former and 2P wakes are observed in the latter. Contours show that these wakes are captured sufficiently in the current implementation.

In order to reveal the energetic structures in the flow field of the pitching plate problem, we conduct a snapshot POD (Proper Orthogonal Decomposition) analysis on the velocity field obtained from simulations. In this analysis, the velocity field is decomposed into mean and fluctuating parts as

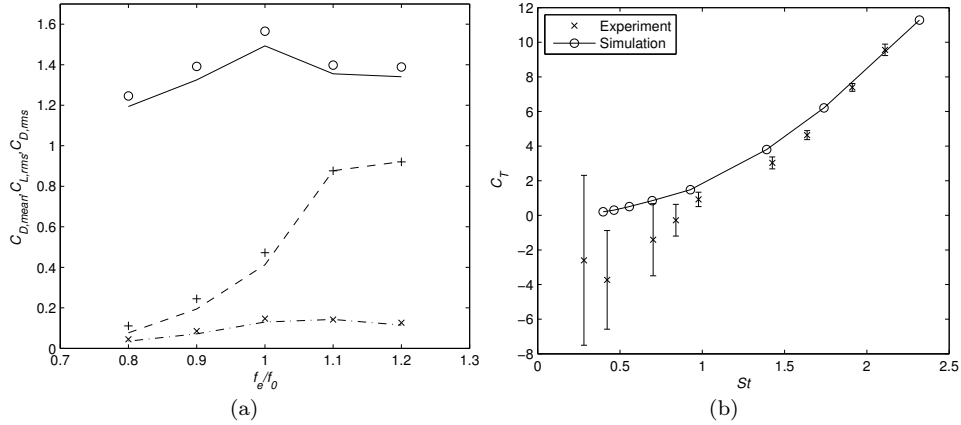


Figure 4: Comparison of mean force coefficients: (a) The oscillating cylinder case at  $Re_D = 185$ . Solid, dashed and dash-dotted lines correspond to  $\bar{C}_D$ ,  $C_{L,rms}$  and  $C_{D,rms}$  from [4], respectively. (b) Experimental and computational time-averaged thrust coefficient for a pitching plate at  $Re_c = 2000$ .

$$\mathbf{V} = \mathbf{V}_m + \mathbf{V}' \quad (16)$$

and the fluctuating part is written as

$$\mathbf{V}'(\mathbf{x}, t) = \sum_{i=1}^M \alpha_i(t) \Phi(\mathbf{x}) \quad (17)$$

An eigenvalue problem in the form of  $\mathbf{CA} = \lambda\mathbf{A}$  is solved to obtain eigenvalues ( $\lambda$ ) and eigenvectors ( $\mathbf{A}$ ) where the entries of the matrix  $\mathbf{C}$  are the inner products  $c_{ij} = (\mathbf{V}'_i, \mathbf{V}'_j)$ . Then the POD modes are found by,

$$\Phi_i = \frac{1}{\sqrt{\lambda_i}} \sum_{j=1}^N A_j^i \mathbf{V}'_j \quad (18)$$

where the  $A_j^i$  is the  $j$ th element of the  $i$ th eigenvector  $\mathbf{A}_i$  [8]. Figure 6 shows the eigenvalues ( $\lambda$ ) obtained from the POD analysis for the pitching plate at  $Re_c = 2000$  and  $St=0.2$ . Results indicate that modes that are comparable in terms of contained energy appear in pairs. Additionally, the accumulation of the energy levels yield that 3 pairs of modes are sufficient to represent the 94 percent of the fluctuating kinetic energy. Mode contours are shown in Figure 7. Mode 1 manifests a structure that is similar to the observed 2S wake.

## 4 Conclusion and Future Work

Selected results of a preliminary validation process of a recently released, open-source based IBM solver has been presented in this work. Results show that the code seems promising, especially for the computational studies in the bio-fluids community. Future work will include more detailed study on the solver such as the assesment of the overall accuracy, comparison of pressure Poisson solvers and a detailed inspection of the spurious force oscillations.

## References

- [1] Rajat Mittal and Gianluca Iaccarino. Immersed boundary methods. *Annu. Rev. Fluid Mech.*, 37:239–261, 2005.

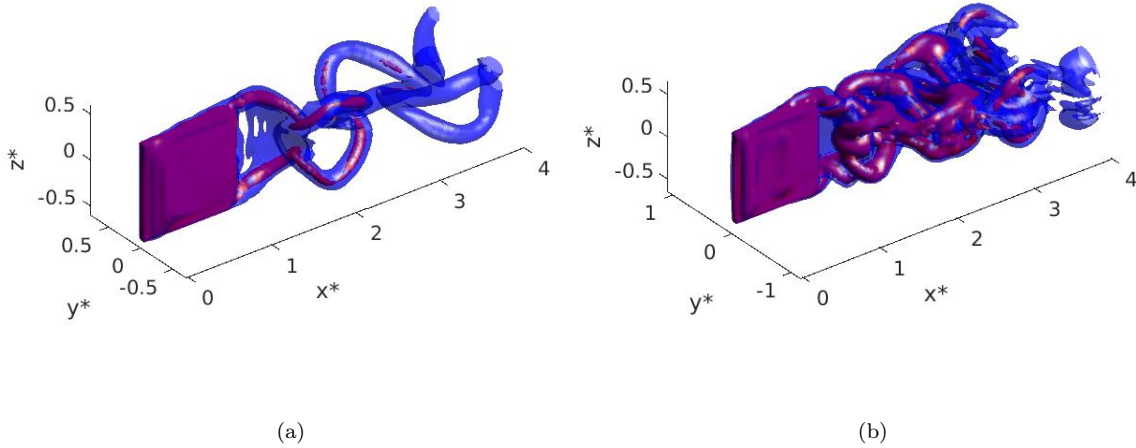


Figure 5: Iso-surfaces of non-dimensional vorticity: (a)  $Re_c = 2000$  and  $St=0.2$ , (b)  $Re_c = 2000$  and  $St=0.4$ .

- [2] Hrvoje Jasak. *Error analysis and estimation for the finite volume method with applications to fluid flows*. PhD thesis, Imperial College London (University of London), 1996.
- [3] Željko Tuković and Hrvoje Jasak. A moving mesh finite volume interface tracking method for surface tension dominated interfacial fluid flow. *Computers & fluids*, 55:70–84, 2012.
- [4] E Guilmineau and P Queutey. A numerical simulation of vortex shedding from an oscillating circular cylinder. *Journal of Fluids and Structures*, 16(6):773–794, 2002.
- [5] Jung Hee Seo and Rajat Mittal. A sharp-interface immersed boundary method with improved mass conservation and reduced spurious pressure oscillations. *Journal of computational physics*, 230(19):7347–7363, 2011.
- [6] Jianming Yang and Elias Balaras. An embedded-boundary formulation for large-eddy simulation of turbulent flows interacting with moving boundaries. *Journal of Computational Physics*, 215(1):12–40, 2006.
- [7] Peter A Dewey, Birgitt M Boschitsch, Keith W Moored, Howard A Stone, and Alexander J Smits. Scaling laws for the thrust production of flexible pitching panels. *Journal of Fluid Mechanics*, 732:29–46, 2013.
- [8] Zongxian Liang and Haibo Dong. On the symmetry of proper orthogonal decomposition modes of a low-aspect-ratio plate. *Physics of Fluids (1994-present)*, 27(6):063601, 2015.

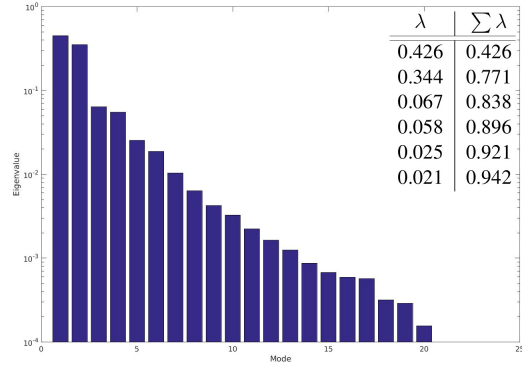


Figure 6: Eigenvalues obtained from the snapshot POD analysis for the plate problem at  $Re_c = 2000$  and  $St=0.2$ .

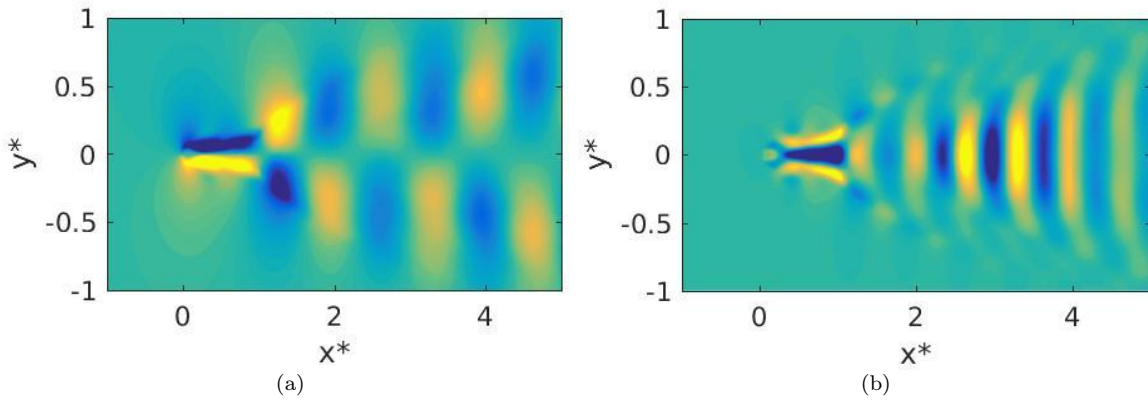


Figure 7: Mode contours at the centerline plane: (a) Mode 1, (b) Mode 3.